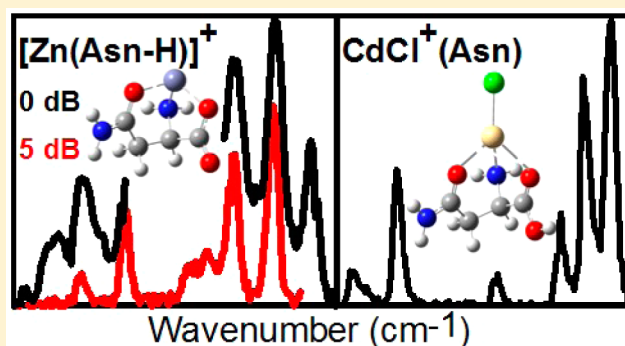


Experimental and Theoretical Investigations of Infrared Multiple Photon Dissociation Spectra of Asparagine Complexes with Zn^{2+} and Cd^{2+} and Their Deamidation Processes

Georgia C. Boles,[†] Rebecca A. Coates,[†] Giel Berden,[‡] Jos Oomens,^{‡,§} and P. B. Armentrout^{*,†}[†]Department of Chemistry, University of Utah, 315 South 1400 East, Room 2020, Salt Lake City, Utah 84112, United States[‡]Radboud University, Institute for Molecules and Materials, FELIX Laboratory, Toernooiveld 7c, NL-6525 ED Nijmegen, The Netherlands[§]van't Hoff Institute for Molecular Sciences, University of Amsterdam, Amsterdam, The Netherlands

Supporting Information

ABSTRACT: Complexes of asparagine (Asn) cationized with Zn^{2+} and Cd^{2+} were examined by infrared multiple photon dissociation (IRMPD) action spectroscopy using light generated from a free electron laser. Electrospray ionization yielded complexes of deprotonated Asn with Zn^{2+} , $[\text{Zn}(\text{Asn}-\text{H})]^+$, and intact Asn with CdCl^+ , $\text{CdCl}^+(\text{Asn})$. Series of low energy conformers for each complex were found using quantum chemical calculations in order to identify the structures formed experimentally. The experimentally obtained spectra were compared to those calculated from optimized structures at the B3LYP/6-311+G(d,p) level for $[\text{Zn}(\text{Asn}-\text{H})]^+$ and the B3LYP/def2-TZVP level with an SDD effective core potential on cadmium for the $\text{CdCl}^+(\text{Asn})$ system. The main binding motif observed for the CdCl^+ complex is a charge solvated, tridentate $[\text{N}, \text{CO}, \text{CO}_2]$ structure where the metal binds to the backbone amino group and carbonyl oxygens of the carboxylic acid and side-chain amide groups. The Zn^{2+} system deprotonates at the backbone carboxylic acid and prefers a $[\text{N}, \text{CO}^-, \text{CO}_2]$ binding motif, where binding was observed at the carboxylate site along with the backbone amino group and side-chain carbonyl groups. In both cases, the theoretically determined lowest-energy conformers explain the experimental $[\text{Zn}(\text{Asn}-\text{H})]^+$ and $\text{CdCl}^+(\text{Asn})$ spectra well. Additionally, complete mechanistic pathways were found for each of the major dissociation reactions of $[\text{Zn}(\text{Asn}-\text{H})]^+$ (primary loss of CO_2 , followed by the sequential loss of NH_3) and $\text{CdCl}^+(\text{Asn})$ (concomitant loss of $\text{NH}_3 + \text{CO}$).



INTRODUCTION

Deamidation at asparagine (Asn) residues is a post translational modification that occurs in proteins and plays an important role in degenerative aging diseases, such as Parkinson's and Alzheimer's.^{1–4} Thus, asparagine containing systems have been studied extensively. In the gas phase, our group has studied complexes of asparagine cationized with Li^+ , Na^+ , K^+ , Rb^+ , Cs^+ , and Ba^{2+} by infrared multiple photon dissociation (IRMPD)⁵ spectroscopy as well as asparagine cationized with H^+ , Na^+ , and K^+ by threshold collision-induced dissociation (TCID) in order to study the structural and energetic characteristics of these complexes.^{6–8} In the present study, IRMPD spectroscopy was utilized to study asparagine cationized with Zn^{2+} and Cd^{2+} , as these two metals play an important role in binding to amino acids under biological conditions, particularly in zinc finger domains.^{9,10} Zn^{2+} binds preferentially to cysteine (Cys) and histidine (His) amino acid sites within proteins, although it is not obvious why those amino acids are preferred. The replacement of Zn^{2+} centers with Cd^{2+} and additional cations has been documented;

however, the nature of the metal dependence of these systems is not yet completely understood.^{11,12} Previous IRMPD studies have evaluated the binding of Zn^{2+} and Cd^{2+} with His,¹³ Cys and CysOMe,¹⁴ Gln,¹⁵ and Ser,¹⁶ thereby elucidating important structural information regarding the metal dependence of these systems. In the current work, we continue this evaluation of amino acid binding to Zn^{2+} and Cd^{2+} , with an additional interest in evaluating the deamidation processes of these Asn complexes.

In order to definitively determine conformations of the $[\text{Zn}(\text{Asn}-\text{H})]^+$ and $\text{CdCl}^+(\text{Asn})$ complexes formed experimentally, IRMPD action spectra for each complex were measured. Experimental spectra are then compared to spectra calculated for a series of low-energy conformers with optimized structures and vibrational frequencies determined at the B3LYP/6-311+G(d,p) or B3LYP/def2-TZVP level of theory,

Received: October 12, 2016

Revised: November 16, 2016

Published: November 17, 2016

where an SDD effective core potential was used for cadmium. Comparison of the calculated and experimental spectra of each system allows for clear identification of the populated conformation of each complex. Theory also provides mechanistic details of the deamidation processes observed. Results presented here provide a great deal of information regarding metal dependence effects with respect to binding affinity, structural characteristics, and deamidation processes. Combined with results of our previous studies, analysis of these complexes allows for a more complete understanding of the metal dependence of other biologically relevant amino acid systems, e.g., the preferential binding to Cys and His.

■ EXPERIMENTAL AND COMPUTATIONAL SECTION

Mass Spectrometry and Photodissociation. Experiments were performed at the free electron lasers for infrared experiments (FELIX) facility of Radboud University in The Netherlands.¹⁷ A 4.7 T Fourier transform ion cyclotron resonance (FT-ICR) mass spectrometer, described elsewhere, was used to measure the IRMPD spectra.^{18–20} Ions were generated using an electrospray ionization (ESI) source and then accumulated in a hexapole trap for about 5 s before being pulse extracted through a quadrupole bender and injected into the ICR cell via a radiofrequency (rf) octopole ion guide. Electrostatic switching of the dc bias of the octopole was used to avoid collisional heating of the ions.¹⁹ Once trapped in the ICR cell, the ion of interest (assumed to be roughly at room temperature) was mass selected using a stored waveform inverse Fourier transform (SWIFT) excitation pulse.^{21,22} These ions were irradiated with FELIX for 2–3 s at a 10 Hz macropulse repetition rate (energy up to 45 mJ per macropulse and a bandwidth of 0.5% of the central frequency). The IRMPD spectra were generated by plotting the photo-fragmentation yield, $Y = \sum I_F / (\sum I_P + \sum I_F)$, where I_P and I_F are the integrated intensities of the parent and fragment ion mass peaks (where the sum includes all isotopes), respectively, as a function of the frequency of IR radiation. The yield is linearly corrected for frequency dependent variation in the laser pulse energy. The application of a linear laser power correction is well described in the literature²³ and is appropriate because the power dependence is basically linear until saturation begins because of the incoherent rather than coherent nature of the multiple photon excitation process. IRMPD fragmentation of the $[\text{Zn}(\text{Asn}-\text{H})]^+$ complex appeared to be saturated at wavenumbers corresponding to the highest intensity bands such that a spectrum with 5 dB attenuation of the laser power was also recorded below 1720 cm^{-1} . Comparable levels of attenuation have been used in studies of similar systems.¹³

Metalated Asn complexes were prepared from solutions of 1.0 mM Asn and 1.0 mM $\text{Zn}(\text{NO}_3)_2$ or CdCl_2 in 60:40 MeOH/ H_2O solvent using a Micromass Z-Spray ESI source. Flow rates of $6 \mu\text{L}/\text{min}$ were used, and the electrospray needle was held at a voltage of 2.4 kV. In the case of the Zn^{2+} complex, the ESI source generated a $[\text{Zn}(\text{Asn}-\text{H})\text{ACN}]^+$ complex, in which the asparagine is deprotonated and ACN = acetonitrile, CH_3CN . (The ACN was present adventitiously from previous experiments.) In this case, a CO_2 laser was used to irradiate the sample for 0.3 s to remove the ACN ligand, leaving the $[\text{Zn}(\text{Asn}-\text{H})]^+$ complex. The resulting ions were mass isolated and allowed to cool radiatively for 0.4 s.²⁴ Electrospray of the Cd^{2+} solution generated $\text{CdCl}^+(\text{Asn})$, which did not dissociate upon CO_2 laser irradiation.

Computational Details. In order to determine low-lying conformers of the cationized Asn complexes, a series of 10–15 unique conformers of Asn were first optimized at the B3LYP/6-311+G(d,p) level, using the Gaussian 09 suite of programs.²⁵ For the $[\text{Zn}(\text{Asn}-\text{H})]^+$ system, each of these structures were deprotonated (all possible sites were explored) and a Zn^{2+} cation was introduced to the system (all reasonable binding sites were explored). For the $\text{CdCl}^+(\text{Asn})$ system, CdCl^+ was added to Asn exploring all possible binding sites. Initial optimizations of the metalated complexes were then done using the “loose” keyword to utilize a large step size of 0.01 au and an rms force constant of 0.0017 to facilitate convergence. Unique structures were then further optimized at the B3LYP/6-311+G(d,p) level of theory for Zn^{2+} complexes and at the B3LYP/def2-TZVP level, where def2-TZVP is a size-consistent basis set for all atoms and includes triple- ζ + polarization functions with a small core (28-electron) effective core potential (ECP) on Cd.^{26,27} The def2-TZVP basis set and corresponding ECP were obtained from the EMSL basis set exchange.²⁸ These combinations of level of theory, basis set, and ECP have previously proven to provide accurate structural information with complexes of similar size and composition.^{13–16} Geometry optimizations of metalated structures were also conducted including corrections for empirical dispersion at the B3LYP-GD3BJ level.²⁹

Vibrational frequencies were calculated at these levels of theory and scaled by 0.975 for comparison to the IRMPD spectra. This scaling factor has been shown to account for known inaccuracies in the calculated frequencies, and therefore gives good agreement with well-resolved peaks in other IRMPD spectra.^{13–16} The calculated frequencies were broadened using a 30 cm^{-1} full width at half-maximum Gaussian line shape when used for comparison to the experimentally determined spectra. This broadening accounts for the finite laser bandwidth, unresolved rotational structure of the ions (which are near room temperature), and anharmonicity of the vibrational mode in combination with broadening as a result of the multiple photon absorption process.³⁰

Relative energies were determined for B3LYP geometries using single point energies calculated at the B3LYP, B3P86, and MP2(full) levels using 6-311+G(2d,2p) (Zn^{2+} complexes) and def2-TZVPP (Cd^{2+} complexes) basis sets. Relative B3LYP-GD3BJ single point energies using these larger basis sets and the B3LYP-GD3BJ geometries were also computed. Zero point energy (ZPE) corrections were applied to single point energies in order to provide 0 K relative enthalpies. Thermal corrections to obtain 298 K Gibbs free energies were calculated as outlined previously from 0 K relative enthalpies by using the rigid rotor/harmonic oscillator approximation with the calculated rotational constants and vibrational frequencies.⁵ Vibrational frequencies were scaled by 0.989 when used for zero point energy (ZPE) and thermal corrections.

■ RESULTS AND DISCUSSION

IRMPD Action Spectroscopy. IRMPD action spectra for the $[\text{Zn}(\text{Asn}-\text{H})]^+$ and $\text{CdCl}^+(\text{Asn})$ complexes are shown in Figure 1, where the main product fragments in each case were used to determine the yield spectrum. Linear corrections of the laser power were applied and result in higher relative intensities of the high frequency bands and minor changes in the low frequency region. In each case, the spectral region was scanned from 5.5 to $10 \mu\text{m}$ (1820 to 1000 cm^{-1}), as there are no unique

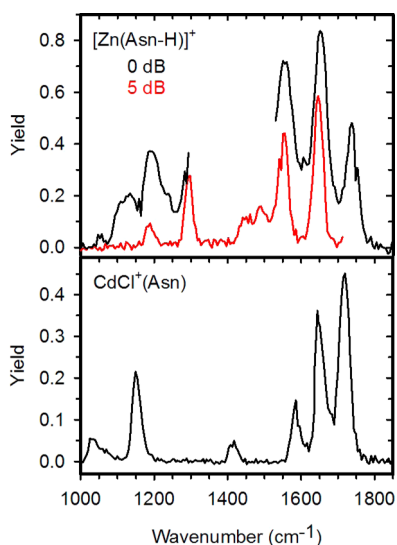
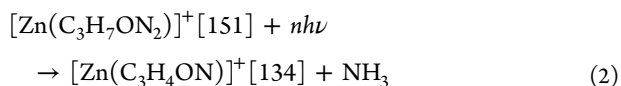
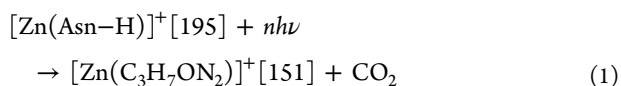


Figure 1. Infrared multiple photon dissociation (IRMPD) action spectra of Zn^{2+} and Cd^{2+} complexes of Asn. Spectra taken with attenuated laser power (in decibels) are indicated in red.

features in lower frequency regions of the theoretically calculated spectra for all low-energy conformers.

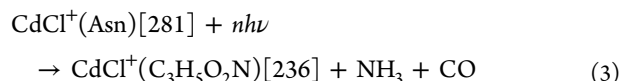
Photodissociation of $[\text{Zn}(\text{Asn}-\text{H})]^+$ and $\text{CdCl}^+(\text{Asn})$ complexes both result in fragments corresponding to deamidation. However, these processes proceed via pathways different from each other and different than those observed in the related glutamine (Gln) systems,¹⁵ as discussed in more detail below. IRMPD of the parent $[\text{Zn}(\text{Asn}-\text{H})]^+$ complex resulted in the fragmentation pattern shown in reactions 1 and 2, where the numbers in brackets indicate the mass to charge ratio of the ion. Because ^{64}Zn is the most abundant isotope (49.17% natural abundance),³¹ the complex of this isotope is designated here as the parent ion. Channels corresponding to ^{66}Zn and ^{68}Zn (27.73 and 18.45% natural abundance, respectively)³¹ were also monitored and included in yield calculations shown in Figure 1.



The major product appears at m/z 151 and results from the loss of CO_2 , reaction 1. As the Asn ligand is deprotonated at the carboxylic acid site, the loss of CO_2 is clearly a reasonable fragment. As shown by reaction 2, deamidation occurs via a secondary loss from m/z 151; however, the m/z 134 product had an intensity not significantly above the noise level (consistent with its identification as a secondary product) and therefore was not included in the measurement of the spectrum. For comparison, $[\text{Zn}(\text{Gln}-\text{H})]^+$ dissociation also resulted in CO_2 loss but was accompanied by Zn loss as well. Then, sequential deamidation occurred, and the deamidation product channel exhibited a much higher intensity.¹⁵

The IRMPD of $\text{CdCl}^+(\text{Asn})$ resulted in one major fragment, as shown in reaction 3. Here, masses are chosen to correspond to the most abundant isotopes of Cd and Cl, ^{114}Cd and ^{35}Cl , such that m/z 281 is designated as the parent ion and $m/z =$

236 as the fragment. The complexes associated with m/z values corresponding to ^{113}Cd , ^{112}Cd , ^{111}Cd , ^{110}Cd , and ^{37}Cl were also monitored and included in yield calculations shown in Figure 1.



The m/z 236 product likely corresponds to the concomitant loss of $(\text{NH}_3 + \text{CO})$ from the Asn ligand, but neither product associated with the possible primary losses was observed, as illustrated in Figure S2. Although the sequence of losses is experimentally indistinguishable, deamidation occurring as the primary loss, followed by sequential dissociation of CO , would be consistent with reaction pathways found for the decomposition of $\text{H}^+(\text{Asn})$ by CID⁸ and $\text{CdCl}^+(\text{Gln})$ by IRMPD.¹⁵ This result will be explored in more detail theoretically below.

Theoretical Results: Relative Energies. Tables S1 and S2 (Supporting Information) give relative single point energies and free energies for conformers of $[\text{Zn}(\text{Asn}-\text{H})]^+$ and $\text{CdCl}^+(\text{Asn})$, respectively, calculated at the B3LYP, B3LYP-GD3BJ, B3P86, and MP2(full) levels of theory (relative to the lowest-energy isomer at each level of theory). Complexes are named using nomenclature outlined previously.¹⁵ In short, the complexes are designated by their metal binding site in brackets, with the deprotonation site (if present) indicated by a negative sign. In most systems, both the backbone and side-chain carbonyls are binding sites with a subscript *s* (for side chain) designating the latter. The designation of the metal binding site is then followed by the amino acid orientation, which is represented by the characterization of dihedral angles as *cis* (*c*, for angles between 0 and 45°), *gauche* (*g*, 45–135°), or *trans* (*t*, 135–180°). In a few cases, signs of the *gauche* angles (+ or -) are also needed in order to distinguish otherwise identical names. Dihedral angles were measured starting from the carboxylic acid hydrogen (unless this site is deprotonated) or the analogous proton on NH_2 in zwitterionic structures and going to the terminal side-chain nitrogen. In cases where deprotonation does not occur at any of the metal binding sites, the deprotonation site is added in parentheses. When deprotonation occurs at a carbon along the backbone, standard nomenclature is used (α , β , γ , ...).

At all levels of theory, the predicted lowest energy $[\text{Zn}(\text{Asn}-\text{H})]^+$ complex adopts a tridentate $[\text{N}, \text{CO}^-, \text{CO}_s]$ binding motif (Figure 2), where the metal binds to the backbone amino group, the carbonyl oxygen of the deprotonated carboxylic acid group, and the carbonyl oxygen of the amide side-chain group. Only one conformation having this binding motif was found, although all other conformers up to 82 kJ/mol across all levels of theory are also characterized as tridentate. Two $[\text{N}^-, \text{CO}, \text{CO}_s]$ conformers (Figure 2) are the next lowest in energy, having relative 0 K energies 39–53 kJ/mol above the ground conformer. The more favorable energetics of the *tg_g+t* conformer appear to be the result of less constrained backbone dihedral angles such that the sum of the $\angle\text{NMO}$ angles of the *tg_g+t* conformer is slightly greater than that of the *tg_g-t* conformer. Two tridentate conformers, $[\text{CO}_2^-, \text{CO}_s]\text{-gcg}$ (Figure 2) and $[\text{CO}_2^-, \text{N}_s]\text{-ggg}$ (not shown), were found where binding takes place at both oxygens of the deprotonated carboxylate group. Here, the possible binding sites at the amide side-chain group have a significant effect on the relative energetics, as the $[\text{CO}_2^-, \text{CO}_s]$ conformer (76–85 kJ/mol relative to the ground conformer) is 56–65 kJ/mol lower in energy than the $[\text{CO}_2^-, \text{N}_s]$ conformer. A similar effect

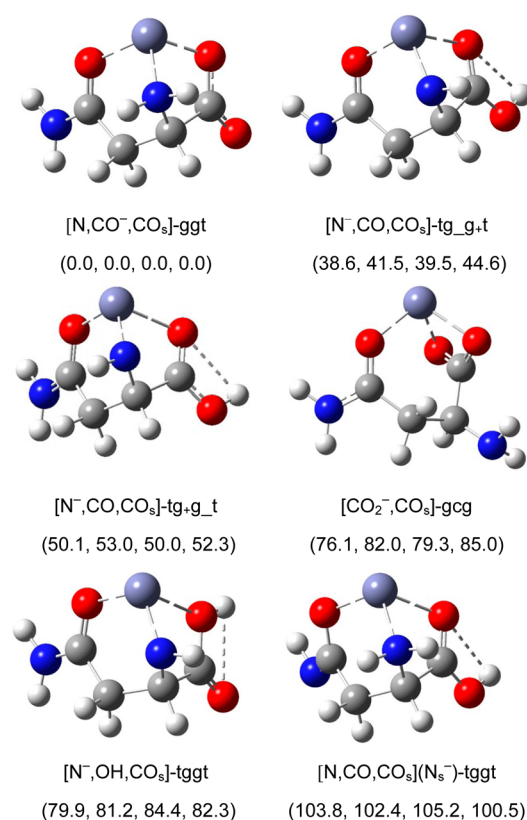


Figure 2. Structures of select $[\text{Zn}(\text{Asn-H})]^+$ conformers calculated at the B3LYP/6-311+G(d,p) level of theory. Relative single point enthalpies (0 K) are given at the B3LYP, B3LYP-GD3BJ, B3P86, and MP2(full) levels, respectively. Short dashed lines indicate hydrogen bonds (up to 2.5 Å). Metal–ligand interactions are shown by long dashed lines.

regarding the specificity of binding at the amide group is observed for the $[\text{N}, \text{CO}^-, \text{N}_s]$ conformers, which lie 71–87 kJ/mol higher than the $[\text{N}, \text{CO}^-, \text{CO}_s]$ ground conformer. Thus, there is much more stability associated with binding at the oxygen of the carbonyl group compared with the amide nitrogen, as also confirmed by the shorter M–O_s distance in the $[\text{N}, \text{CO}^-, \text{CO}_s]$ conformer (1.96 Å) compared with the M–N_s distances in the $[\text{N}, \text{CO}^-, \text{N}_s]\text{-g_g_g_g}$ and $[\text{N}, \text{CO}^-, \text{N}_s]\text{-g_g_g_g}$ conformers (2.09 and 2.06 Å, respectively). Notably, one tridentate conformer was found where binding takes place at a deprotonated carbon of the backbone chain, $[\text{N}, \text{CO}, \text{C}_\gamma^-]\text{-tggt}$, which has relative energies 104–111 kJ/mol higher than the ground conformer. Three conformers where deprotonation occurs at the amide nitrogen, $[\text{N}, \text{CO}, \text{CO}_s](\text{N}_s^-)$, were found, where the lowest energy conformer of this type, $[\text{N}, \text{CO}, \text{CO}_s](\text{N}_s^-)\text{-tg_g_t}$, is shown in Figure 2.

Several bidentate binding motifs were also found for $[\text{Zn}(\text{Asn-H})]^+$ with relative energies 83–251 kJ/mol higher in energy than the ground conformer, clearly indicating an increased stability with the tridentate conformers. The two lowest energy bidentate conformers have similar relative energies (83–95 kJ/mol higher than the ground conformer) and involve binding at the carbonyl of the amide side chain coupled with either the deprotonated backbone carbonyl or amino sites. The highest energy $[\text{Zn}(\text{Asn-H})]^+$ conformer, $[\text{CO}_2^-]\text{-ctg}$ (175–251 kJ/mol above the ground conformer), is also characterized by a bidentate binding motif where binding only takes place at both oxygens of the carboxylate group.

Similar to the $[\text{Zn}(\text{Asn-H})]^+$ conformers, the lowest energy $\text{CdCl}^+(\text{Asn})$ conformer is characterized by a $[\text{N}, \text{CO}, \text{CO}_s]$ binding motif (Figure 3). This is similar to what is observed in other amino acid systems.^{5,15,16,32–34} The next four lowest energy conformers lie within ~40 kJ/mol of the ground conformer, but only one of those conformers, $[\text{N}, \text{OH}, \text{CO}_s]\text{-tggt}$, is characterized by a tridentate binding motif. One zwitterionic form of $\text{CdCl}^+(\text{Asn})$, $[\text{CO}_2^-]\text{-ctgt}$, was found to be only 20–32 kJ/mol higher than the ground conformer, and is stabilized by NH–OC and NH–OC_s hydrogen bonds (Figure 3). This zwitterionic binding motif was also found to be a low-energy conformer of Asn cationized with Li^+ , Na^+ , K^+ , Rb^+ , Cs^+ , and Ba^{2+} ,⁵ as well as Gln complexes cationized with Zn^{2+} and Cd^{2+} ,¹⁵ and Li^+ , Na^+ , K^+ , and Cs^+ .³² We also find that $[\text{N}, \text{CO}_s]\text{-tggt}$ is 5–8 kJ/mol lower in energy than $[\text{N}, \text{CO}]\text{-tggt}$. This is consistent with previous TCID studies which concluded that the Na^+ binding affinity to Gln (with an amide side chain) is ~15 kJ/mol higher than that to Glu (with a carboxylic acid side chain), a direct result of lower charge withdrawal by the NH₂ amide group compared to the OH hydroxyl group. Another consideration here is that $[\text{N}, \text{CO}_s]\text{-tggt}$ forms a six-membered ring at the complexation site, whereas $[\text{N}, \text{CO}]\text{-tggt}$ forms a five-membered ring. Comparable to the $[\text{Zn}(\text{Asn-H})]^+$ conformers, $\text{CdCl}^+(\text{Asn})$ conformers exhibit a strong specificity for binding to the carbonyl of the amide side chain. Namely, the $[\text{N}, \text{CO}, \text{N}_s]$ conformer is 50–60 kJ/mol higher in energy than the $[\text{N}, \text{CO}, \text{CO}_s]$ ground conformer, nearly equivalent to the analogous increase in energy observed with the $[\text{Zn}(\text{Asn-H})]^+$ conformers.

Theoretical Results: $[\text{Zn}(\text{Asn-H})]^+$ Structures. A full description of the key geometric parameters of each major identified binding motif for the $[\text{Zn}(\text{Asn-H})]^+$ conformers is given in Table S3 (Supporting Information), where our structural analysis provides a great deal of information on the binding affinity and conformational effects of these complexes.

As stated above, only one conformer of the $[\text{N}, \text{CO}^-, \text{CO}_s]$ binding motif was located for the $[\text{Zn}(\text{Asn-H})]^+$ complex, the $[\text{N}, \text{CO}^-, \text{CO}_s]\text{-ggt}$ ground conformer. Here, deprotonation occurs at the carboxylic acid site, as is also found for $[\text{N}, \text{CO}^-, \text{N}_s]$, $[\text{CO}^-, \text{CO}_s]\text{-ggg}$, and $[\text{N}, \text{CO}^-]$. All of these conformers are characterized by relatively short M–O distances, ranging from 1.81 to 1.89 Å, where the shortest distance is observed in the bidentate $[\text{CO}^-, \text{CO}_s]$. Likewise, conformers where deprotonation occurs at the amino nitrogen ($[\text{N}^-, \text{CO}, \text{CO}_s]$, $[\text{N}^-, \text{OH}, \text{CO}_s]$, $[\text{N}^-, \text{CO}_s]$, and $[\text{N}^-, \text{CO}, \text{N}_s]$) exhibit the shortest M–N distances, 1.85–1.90 Å. The longest M–N distances are observed in conformers where deprotonation occurs at the amide group, $[\text{N}, \text{CO}, \text{CO}_s^-]$, and in one instance, at a carbon of the backbone, $[\text{N}, \text{CO}, \text{C}_\gamma^-]$. Other notable comparisons arise from examining the M–O distances in $[\text{N}^-, \text{CO}, \text{CO}_s]$ conformers (2.14–2.18 Å), which are much shorter than the M–O distance in the analogous $[\text{N}^-, \text{OH}, \text{CO}_s]$ conformer (2.37 Å). This stronger interaction leads to favorable energetics of the $[\text{N}^-, \text{CO}, \text{CO}_s]$ conformers, 33–41 kJ/mol lower in energy than $[\text{N}^-, \text{OH}, \text{CO}_s]\text{-tggt}$. Likewise, the M–N and M–O distances are very similar for the $[\text{N}, \text{CO}^-, \text{CO}_s]\text{-ggt}$ and $[\text{N}, \text{CO}^-, \text{N}_s]\text{-g_g_g_g}$ conformers (the lowest energy conformers of each type), although the M–Y_s distance increases by about 0.1 Å when the carbonyl binding site is replaced with the amide nitrogen.

A few trends were also observed in the $\angle \text{XMO}$, $\angle \text{XMY}_s$, and $\angle \text{OMY}_s$ angles. Of the tridentate $[\text{Zn}(\text{Asn-H})]^+$ complexes,

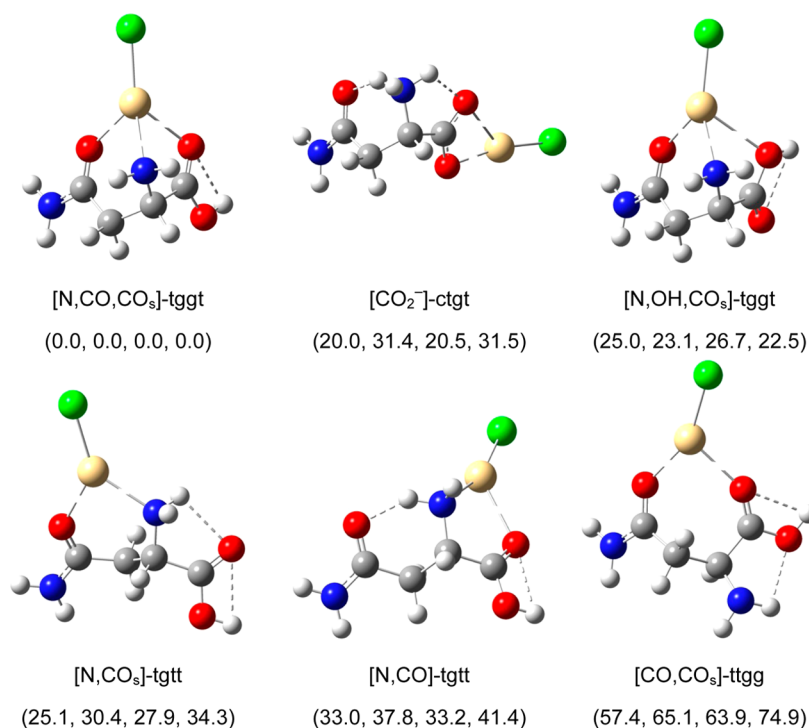


Figure 3. Structures of low-energy $CdCl^+(Asn)$ conformers calculated at the B3LYP/def2-TZVP level of theory. Relative single point enthalpies (0 K) in kJ/mol are given at the B3LYP, B3LYP-GD3BJ, B3P86, and MP2(full) levels, respectively. Short dashed lines indicate hydrogen bonds (up to 2.5 Å). Metal–ligand interactions are shown by long dashed lines.

the $[N, CO, C_\gamma^-]-tggt$ conformer exhibits the smallest $\angle NMO$, 78.6° . The next smallest angles were observed with those involving deprotonation at the amide site (78.7 – 81.5°). Here, the more constrained $\angle NMO$ angles, in addition to other factors, clearly have effects on the energetics of these conformers (100–126 kJ/mol above the ground conformer). The bidentate conformers, specifically $[N^-, CO_s]-tttt$, $[N^-, CO_s]-cgtg$, and $[N, N_s^-]-tggt$, have the largest $\angle NMY_s$ angles (111, 114, and 116° , respectively). Although these conformers are clearly less constrained with respect to these angles and have relatively short M–N and M–O distances (indicative of tight binding), the presence of the additional binding site in the tridentate conformations is clearly important, as these bidentate conformers are 84–122 kJ/mol higher in energy than the tridentate ground conformer.

Theoretical Results: $CdCl^+(Asn)$ Structures. Table S4 (Supporting Information) lists the key geometric parameters of major binding motifs for the $CdCl^+(Asn)$ conformers. All $CdCl^+(Asn)$ complexes exhibit longer M–O and M–O_s distances than the $[Zn(Asn-H)]^+$ complexes characterized by a similar binding motif. This reflects the smaller ionic radius of Zn^{2+} (0.60 Å) as compared to that of Cd^{2+} (0.78 Å), as well as tighter binding in the $[Zn(Asn-H)]^+$ complexes as a result of stronger electrostatic interactions between the metal center and deprotonated anion ligand as compared with the intact amino acid in the Cd^{2+} complexes. Here, M–N distances are ~ 0.3 Å longer than those in comparable $[Zn(Asn-H)]^+$ complexes, where this effect is mainly a result of the ionic radius, coupled with tighter binding of the anionic ligand as described above. Similar to the $[Zn(Asn-H)]^+$ system, there was only one conformer having the $[N, CO, CO_s]$ binding motif for the $CdCl^+(Asn)$ conformers, $[N, CO, CO_s]-tggt$. Along with $[N, OH, CO_s]-tggt$ and $[N, CO, N_s]-tggt$, these tridentate conformers exhibit the longest M–N distances (2.37, 2.32,

and 2.34 Å, respectively). Understandably, the shortest M–N distances of the $CdCl^+(Asn)$ conformers are observed in the bidentate conformations, with the $[N, OH]-tggt$ conformer having the shortest distance, 2.18 Å. The longest M–O distances result from binding at the hydroxyl oxygen ($[N, OH, CO_s]$, $[N, OH]$, and $[OH, CO_s]$) as compared with the alternative carbonyl oxygen as observed in the ground conformer. Clearly, there are stronger electrostatic interactions when binding the carbonyl to the metal center.

Interestingly, the M–N, M–O_s, and $\angle NMO_s$ geometric parameters do not differ significantly for the $[N, OH, CO_s]-tggt$ and $[N, CO_s]-tggt$ conformers, where the specified distances are within 0.04 Å and the angles agree within 3° . These structural similarities also result in very comparable energetics, as the bidentate conformer is only 0.1–12 kJ/mol higher in energy than the $[N, OH, CO_s]$ complex, a much smaller energetic penalty than observed in the $[Zn(Asn-H)]^+$ system where bidentate complexes systematically had a much higher relative energy than the ground conformer. A much more noticeable difference between comparable bidentate and tridentate structures for the $CdCl^+(Asn)$ system is observed between the $[N, CO, CO_s]-tggt$ and $[N, CO_s]-tggt$ conformers. Here, the differences between M–N and M–O_s distances and $\angle NMO_s$ were larger, 0.05 Å, 0.09 Å, and 7° , respectively. The energetic cost associated with removing one of the binding sites is also more obvious, as the $[N, CO_s]$ conformer is 25–34 kJ/mol higher in energy than the $[N, CO, CO_s]$ ground conformer.

Comparison of Experimental and Theoretical IR Spectra: $[Zn(Asn-H)]^+$. In comparing the experimental and theoretical IR spectra, it should be remembered that the experimental IRMPD intensities are not always reproduced by the calculated linear absorption spectrum; however, infrared spectra obtained using IRMPD methods are generally

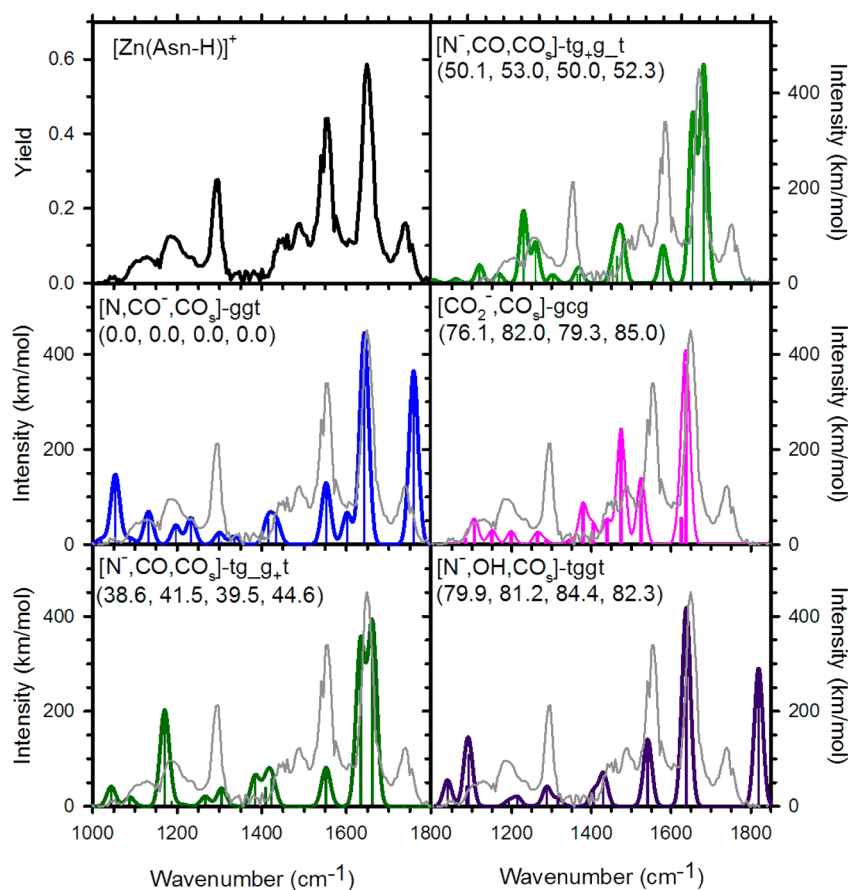


Figure 4. Comparison of the $[\text{Zn}(\text{Asn-H})]^+$ experimental IRMPD action spectrum with IR spectra calculated at the B3LYP/6-311+G(d,p) level of theory for low-lying conformers. Relative 0 K enthalpies (kJ/mol) are given at the B3LYP, B3LYP-GD3BJ, B3P86, and MP2(full) levels, respectively.

comparable to those recorded using linear absorption techniques, in part because the spectra result from incoherent, rather than coherent, multiple photon excitation. Previous modeling studies have demonstrated the near-linear absorption character of IRMPD studies.^{30,35}

As shown in Figure 4, the most intense spectral features in the computed spectra of the lowest energy $[\text{N}, \text{CO}^-, \text{CO}_s]\text{-ggt}$ conformer correlate fairly well with those observed in the experimental $[\text{Zn}(\text{Asn-H})]^+$ spectrum. Here, we have combined the 0 and 5 dB experimental spectra for ease of comparison to the calculated spectra, where clearly the composite spectrum is dominated by the 0 dB contributions at high and low frequencies, with bands from 1300–1500 cm^{-1} indicative of the 5 dB contribution to the spectrum. The bands observed at 1552 (amide CO stretch), 1647 (amide NH_2 bend), and 1738 cm^{-1} (stretch of uncoordinated CO in carboxylate) are consistent with those calculated for the $[\text{N}, \text{CO}^-, \text{CO}_s]\text{-ggt}$ conformer. Here, the most intense band (1647 cm^{-1}) is reproduced very well in frequency and intensity by the calculated spectrum, although the band corresponding to the CO stretch of the carboxylate is blue-shifted by about 20 cm^{-1} compared with the experimental spectrum. However, the $[\text{N}, \text{CO}^-, \text{CO}_s]\text{-ggt}$ species is the only low-lying conformer that exhibits a carboxylate CO stretch in this region. Here, the weak band at 1600 cm^{-1} in the calculated spectrum for the $[\text{N}, \text{CO}^-, \text{CO}_s]\text{-ggt}$ conformer was not explicitly resolved experimentally, although there is a small shoulder present at 0 dB. This band correlates to the NH_2 bend of the backbone amino group and characteristically exhibits a red shift of about

25 cm^{-1} as a result of the strong anharmonic nature of this vibrational mode.^{15,36–41} A similar shift would produce a peak at 1575 cm^{-1} that would overlap with the band at 1552 cm^{-1} , thus accounting for the difference in experimental and theoretical intensities.

There is also reasonable agreement between the experimental and $[\text{N}, \text{CO}^-, \text{CO}_s]\text{-ggt}$ calculated spectra in the lower frequency region. For the experimental/calculated spectra, bands were located at (1053/1053 cm^{-1} , amino NH_2 wagging), (1131/1130 cm^{-1} , amino NH_2 twisting, with minor backbone motions), (1185/1196 cm^{-1} , primarily backbone CH_2 twisting), (1238/1230 cm^{-1} , backbone CCH bending with minor contributions from coordinated CO stretching), (1292/1296 cm^{-1} , amino NH_2 twisting), and (1449/1434 and 1414 cm^{-1} , amide NOC bending with backbone CH_2 wagging). Of these bands, the peaks located at 1131, 1238, and 1292 cm^{-1} all have experimental intensities much higher than predicted theoretically. Likewise, the bands at 1053, 1185, and 1449 cm^{-1} were all calculated to be either comparable or higher in intensity than is observed experimentally. The only spectral feature of the experimental $[\text{Zn}(\text{Asn-H})]^+$ spectrum that is not reproduced in the calculated spectra is the band at 1490 cm^{-1} , a discrepancy for which we have no ready explanation, although a band shifted by anharmonic effects is one possibility.

The calculated spectra for four additional conformers are also given in Figure 4. The $[\text{N}^-, \text{CO}, \text{CO}_s]$ conformers were found to have two intense spectral features centered about the band at 1647 cm^{-1} of the experimental spectrum but did not reproduce the 1738 cm^{-1} band associated with CO stretching of the

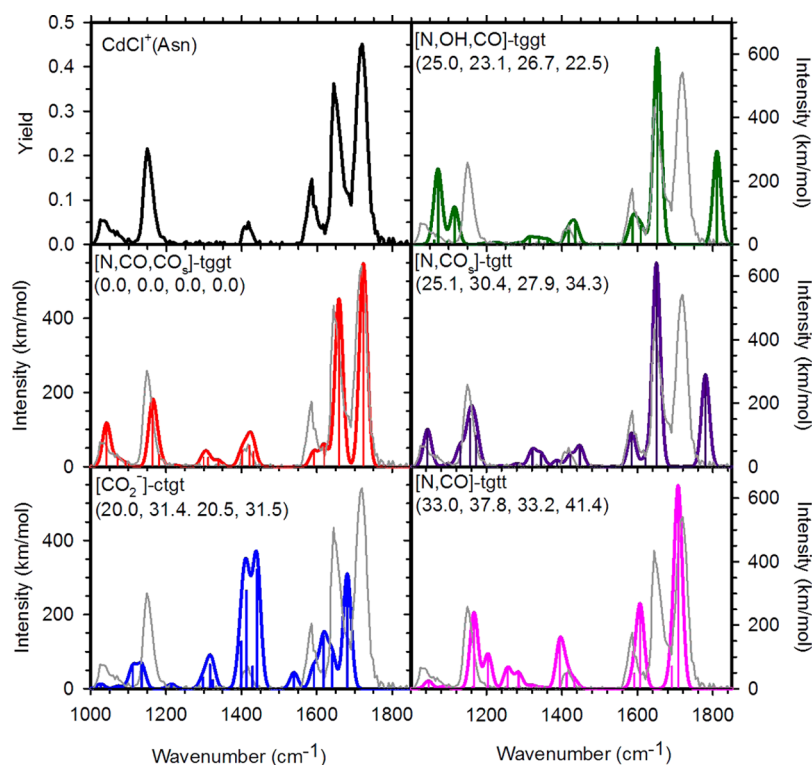


Figure 5. Comparison of the $\text{CdCl}^+(\text{Asn})$ experimental IRMPD action spectrum with IR spectra calculated at the B3LYP/def2-TZVP level of theory for low-lying conformers. Relative 0 K enthalpies (kJ/mol) are given at the B3LYP, B3LYP-GD3BJ, B3P86, and MP2(full) levels, respectively.

deprotonated carboxylic acid (because deprotonation is occurring at the amino nitrogen). Interestingly, $[\text{CO}_2^-, \text{CO}_s]\text{-gcg}$ was the only conformer that exhibits a band in the region where the 1490 cm^{-1} peak is observed in the experimental spectrum. Again, this conformer does not reproduce the CO stretching band observed in the experimental spectrum. $[\text{N}^-, \text{OH}, \text{CO}_s]\text{-tggt}$, the only additional conformer shown that exhibits a CO stretch in the high frequency region, is characterized by a blue-shift by $\sim 80\text{ cm}^{-1}$ with respect to the experimental band at 1738 cm^{-1} , Figure 4.

Therefore, the experimental spectrum appears to be most consistent with the calculated spectrum for $[\text{N}, \text{CO}^-, \text{CO}_s]\text{-ggt}$, the predicted lowest energy $[\text{Zn}(\text{Asn}-\text{H})]^+$ conformer. In addition to a spectral comparison, the probability that $[\text{N}, \text{CO}^-, \text{CO}_s]\text{-ggt}$ was the conformer formed experimentally was also assessed on the basis of an equilibrium distribution of conformers. According to the calculated free energies at all levels of theory, the $[\text{N}, \text{CO}^-, \text{CO}_s]\text{-ggt}$ conformer would have a population of $\geq 99.99\%$ at 298 K.

Comparison of Experimental and Theoretical IR Spectra: $\text{CdCl}^+(\text{Asn})$. Similar to the Zn^{2+} system, the experimental IRMPD action spectrum of $\text{CdCl}^+(\text{Asn})$ is predicted very well by the lowest-energy conformer, $[\text{N}, \text{CO}, \text{CO}_s]\text{-tggt}$; see Figure 5. The main spectral features of the $\text{CdCl}^+(\text{Asn})$ spectrum are observed at 1040, 1149, 1417, 1586, 1644, and 1720 cm^{-1} . Computed bands at 1721 (coordinated CO stretch of the carboxylic acid) and 1656 cm^{-1} (CO stretch of the amide group, with contributions from amide NH_2 bending) reproduce the experimental spectrum extremely well in frequency (shifts within $\sim 10\text{ cm}^{-1}$) and intensity, and are probably the most diagnostic. The remaining bands computed at 1412 (backbone CH_2 bending with minor contributions from COH bending and CNH bending), 1161

(primarily COH bending with a small contribution from NH_2 rocking), and 1038 cm^{-1} (amino NH_2 wagging) all exhibit comparable behavior to the experimental spectrum, with the only significant deviation in frequency being the band at 1161 cm^{-1} , which is blue-shifted by $\sim 10\text{ cm}^{-1}$.

Additionally, for the $[\text{N}, \text{CO}, \text{CO}_s]\text{-tggt}$ conformer, there is a predicted band near 1610 cm^{-1} corresponding to the NH_2 bend of the backbone amino group that is not clearly observed in the experimental spectrum at that frequency. As mentioned above, this effect has been seen in similar systems where it was concluded that strong anharmonic effects red shift the NH_2 band in all cases. A red shift of the same magnitude shown in previous studies would produce a peak at $\sim 1585\text{ cm}^{-1}$ in the $[\text{N}, \text{CO}, \text{CO}_s]\text{-tggt}$ spectrum, thus overlapping the predicted band at 1594 cm^{-1} . A combination of both bands in this frequency range would explain why the peak at 1586 cm^{-1} in the experimental spectrum exhibits a higher relative intensity compared with the predicted spectrum.

Figure 5 shows spectra for an additional four low-lying structures (20–41 kJ/mol higher than the lowest-energy conformer), but the spectral features exhibited in those cases do not match the observed $\text{CdCl}^+(\text{Asn})$ spectrum to a degree that would suggest any of these conformers were formed experimentally. Specifically, the main spectral features in the zwitterionic $[\text{CO}_2^-\text{-ctgt}]$ conformer (20–32 kJ/mol higher than the lowest-energy conformer) are intense bands at 1409 and 1436 cm^{-1} for which there is only a very weak band in the experimental spectrum. All other spectral features do not correspond to any bands present in the $\text{CdCl}^+(\text{Asn})$ spectrum. The only additional tridentate conformer shown, $[\text{N}, \text{OH}, \text{CO}_s]\text{-tggt}$, only reproduces two of the major high frequency bands (those at 1586 and 1644 cm^{-1}). The absence of the predicted band at 1810 cm^{-1} and the failure to reproduce

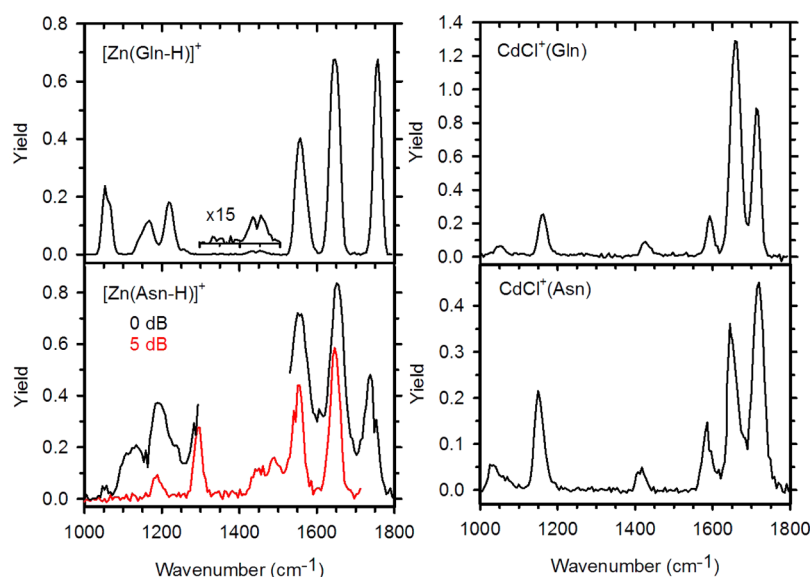


Figure 6. Infrared multiple photon dissociation (IRMPD) action spectra of Zn^{2+} and Cd^{2+} complexes with Asn and Gln.¹⁵

any lower frequency features clearly suggest this conformer is not being formed experimentally. Of the two bidentate conformers shown, $[\text{N}, \text{CO}_s]\text{-tggt}$ reproduces all bands present in the experimental spectrum with the exception of the coordinated CO stretch of the carboxylic acid, as no binding at that site occurs in this conformer. Instead, a blue shift of $\sim 60 \text{ cm}^{-1}$ is observed for the CO stretching band in this spectrum, which is clearly not observed experimentally.

Here, the spectral analysis indicates that solely $[\text{N}, \text{CO}, \text{CO}_s]\text{-tggt}$ is present experimentally, consistent with theoretical calculations at all levels of theory. This conclusion also agrees with an equilibrium distribution of conformers at 298 K, which suggests the $[\text{N}, \text{CO}, \text{CO}_s]\text{-tggt}$ conformer would have a population $\geq 99.99\%$.

Overall Comparison. Here we find it useful to give a more comprehensive analysis of the spectral features exhibited in both the $[\text{Zn}(\text{Asn-H})]^+$ and $\text{CdCl}^+(\text{Asn})$ IRMPD action spectra. As shown in Figures 1, 4, and 5, the main spectral features in the $[\text{Zn}(\text{Asn-H})]^+$ complex are observed at 1053 (0 dB), 1131 (0 dB), 1185, 1292, 1449, 1490, 1552, 1647, and $1738 (0 \text{ dB}) \text{ cm}^{-1}$, whereas those in the $\text{CdCl}^+(\text{Asn})$ spectrum appear at 1040, 1149, 1422, 1586, 1644, and 1720 cm^{-1} . Of the three most intense and diagnostic peaks of the $[\text{Zn}(\text{Asn-H})]^+$ and $\text{CdCl}^+(\text{Asn})$ spectra, the amide NH_2 bending mode at 1647 and 1644 cm^{-1} , respectively, shifts very little. This is a reasonable observation given the same side-chain amide functionality and the fact that metal dependent effects should be minimal, as there is no complexation at this site. In contrast, the CO stretch of the amide experiences a large shift (from 1552 cm^{-1} for the Zn^{2+} complex to 1586 cm^{-1} for the Cd^{2+} complex). Here, the larger shift likely results from more significant perturbations caused by differences in the metal cation binding strength. This can be directly related to the size of the metal center, as smaller metals allow shorter M–O and M–X distances, which translates into stronger electrostatic interactions between the metal and amino acid ligand. Interestingly, this blue shifting of the Cd^{2+} complex (relative to the Zn^{2+} complex) is consistent with previous studies of alkali metal cation complexes with Asn,⁵ although a much larger shift is observed in the current study. This is likely a result of the much stronger M–L interactions in the Zn^{2+} and Cd^{2+} Asn

complexes as compared to those for the singly charged alkali metal complexes. A smaller shift of 18 cm^{-1} in the opposite direction is observed for the CO stretch of the carboxylic acid, from 1738 to 1720 cm^{-1} . The CO band from the stretching of the carboxylate group in the Zn^{2+} spectrum lies above that in the Cd^{2+} spectrum (opposite of what was observed in our previous Asn IRMPD study of alkali metal complexes),⁵ an effect that can be attributed primarily to deprotonation at the carboxylic site in $[\text{Zn}(\text{Asn-H})]^+$. The analogous effect was previously observed in a study of His and Gln complexes of Zn^{2+} and Cd^{2+} where the shift is about 40 cm^{-1} .^{13,15}

Spectral Comparison to $\text{Zn}^{2+}/\text{Cd}^{2+}$ Gln. The IRMPD spectra for $[\text{Zn}(\text{Gln-H})]^+$ and $\text{CdCl}^+(\text{Gln})$ have been measured previously.¹³ Figure 6 shows the comparison between those spectra and the spectra measured for $[\text{Zn}(\text{Asn-H})]^+$ and $\text{CdCl}^+(\text{Asn})$ in the current study. It is clear that the spectra for each metal agree closely with one another, as expected given the same side-chain functionality. For the $[\text{Zn}(\text{Gln-H})]^+$ and $[\text{Zn}(\text{Asn-H})]^+$ complexes, two of the three major diagnostic peaks are nearly identical in frequency (1557 and 1552 cm^{-1} , amide CO stretch) and (1647 and 1647 cm^{-1} , amide NH_2 bend), and only the CO stretch of the carboxylate group experiences a larger shift ($\sim 20 \text{ cm}^{-1}$). The opposite correlation is observed for the Cd^{2+} systems, where the frequency shifts are more evident at the amide CO stretching (1597 and 1586 cm^{-1}) and NH_2 bending (1662 and 1644 cm^{-1}) bands in the $\text{CdCl}^+(\text{Gln})$ and $\text{CdCl}^+(\text{Asn})$ spectra, respectively. Interestingly, all other bands that are represented in both Asn and Gln systems are red-shifted in the Asn spectra by $10\text{--}42 \text{ cm}^{-1}$ (with the only exception being the band at 1053 cm^{-1} in both the $[\text{Zn}(\text{Gln-H})]^+$ and $[\text{Zn}(\text{Asn-H})]^+$ spectra). This red shifting is consistent with previous studies, which have concluded that Asn absorbs $\sim 10 \text{ cm}^{-1}$ lower than Gln as a result of the slightly different environments in which intramolecular interactions (hydrogen bonding) occur.⁴² Specifically, previous theoretical and experimental studies revealed that, as hydrogen bonds weaken (and lengthen), there is typically an associated red shift.⁴³ On the basis of these conclusions, it appears that the additional carbon present in the Gln backbone affects the hydrogen bonding environment sufficiently that corresponding bands in the Asn and Gln spectra (other than the high-

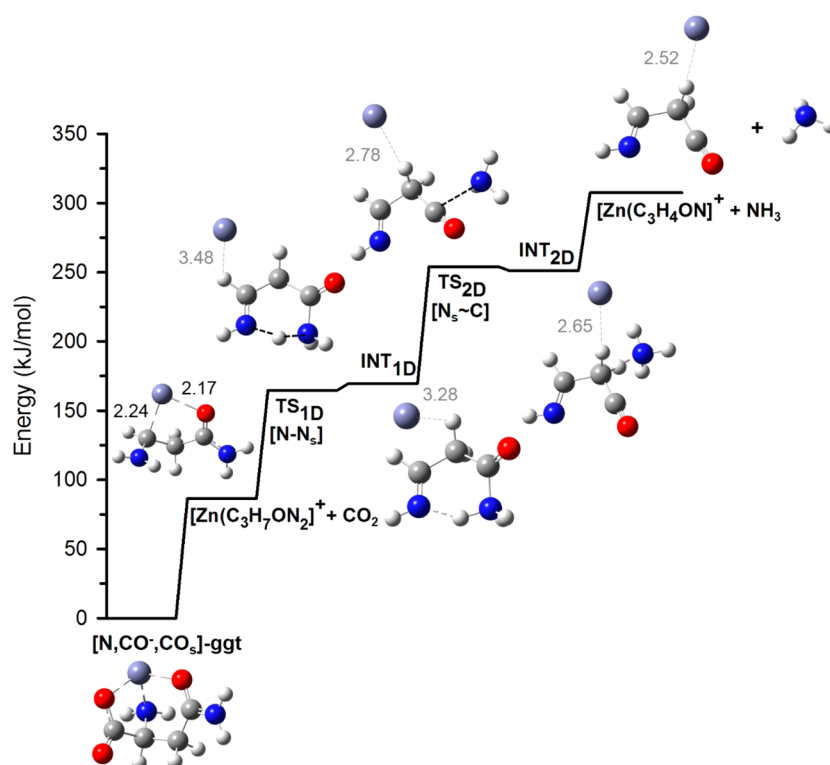


Figure 7. Reaction coordinate for deamidation from $[\text{Zn}(\text{C}_3\text{H}_7\text{ON}_2)]^+$ calculated at the MP2(full)/6-311+G(2d,2p) level of theory, using B3LYP/6-311+G(d,p) geometry optimizations. Structures for intermediates lie below the reaction coordinate, and those for TSs lie above. Long dashed lines (gray) indicate M–L bonds. Dotted lines (black) indicate bonds being broken or formed for transition states. Short dashed lines (gray) indicate hydrogen bonds (up to 2.5 Å). M–L bond lengths (in Å) are given in black and gray for Zn^{2+} –L and Zn–L interactions, respectively.

frequency region discussed above) of Figure 6 are red-shifted in the $[\text{Zn}(\text{Asn}-\text{H})]^+$ and $\text{CdCl}^+(\text{Asn})$ spectra compared to spectra for the analogous Gln complexes.

Interestingly, the band at $\sim 1300\text{ cm}^{-1}$ in the $[\text{Zn}(\text{Asn}-\text{H})]^+$ spectrum is not observed in the Gln system with any significant intensity, although the lowest energy conformers of both systems are predicted to have a band in this region, which is due to backbone CH_2 and amino NH_2 motions. There are indeed two weak bands in the predicted $[\text{Zn}(\text{Asn}-\text{H})]^+$ $[\text{N}, \text{CO}^-, \text{CO}_s]$ -ggt spectrum (CH_2 wagging and CH_2 rocking), see Figure 4, which likely explain the observed intensity. The Gln system is only predicted to have one band (a combination of CH_2 wagging and rocking) near this frequency. Interestingly, this band also appears to be metal dependent, as it is not observed in the $\text{CdCl}^+(\text{Asn})$ spectrum. Furthermore, this band was not observed in Asn or Gln complexes with Li^+ , was observed with only moderate intensity with Na^+ , and was observed with the highest intensity with Cs^+ .^{5,32}

Deamidation Pathways for $[\text{Zn}(\text{Asn}-\text{H})]^+$. Under biological conditions, the mechanism for deamidation of Asn residues is believed to occur via formation of a five-membered cyclic succinimide intermediate.⁴ Because the $[\text{Zn}(\text{Asn}-\text{H})]^+$ complex has been deprotonated at the carboxylic acid, deamidation of this complex cannot occur readily via the same pathway and likely requires more intramolecular rearrangement. It has also been shown experimentally and theoretically that conformational and steric effects play obvious roles in controlling the rate of ring closure, which requires the transfer of a hydrogen to the amide NH_2 to form the NH_3 leaving group. Interestingly, both Asn complexes studied here exhibited dissociation patterns that suggest deamidation is

occurring while the metal center still participates in binding, whereas different behavior was observed with Gln complexes with Zn^{2+} .¹⁵ Thus, the structural and spectral analysis of these complexes is an important factor in evaluating the deamidation properties of these and other biologically relevant systems, specifically in comparison with the Gln complexes of Zn^{2+} .¹⁵

The complete mechanistic pathways for the major dissociation reactions 1–3 were evaluated, with a particular interest in the deamidation processes. Here, the distinction between ammonia loss via the amino or amide group is particularly important, because the deamidation process has been thoroughly documented as being detrimental to protein health.⁴ Thus, we have evaluated the complete mechanistic pathways for each of the possible dissociation processes leading to m/z 134, where the reaction coordinates for deamidation (amide NH_3 loss) and deamination (amino NH_3 loss) from $[\text{Zn}(\text{C}_3\text{H}_7\text{ON}_2)]^+$ are given in Figures 7 and 8, respectively. Optimized B3LYP/6-311+G(d,p) structures of the major dissociation species are given, and relative single point energies given at the B3LYP, B3LYP-GD3BJ, B3P86, and MP2(full) levels of theory are given in Table 1. The starting structure for each of these pathways, $[\text{Zn}(\text{C}_3\text{H}_7\text{ON}_2)]^+$, was found via simple C–C bond cleavage, resulting in the loss of the carboxylate group (CO_2) from the $[\text{N}, \text{CO}^-, \text{CO}_s]$ -ggt lowest energy conformer. Additional higher energy conformers of $[\text{Zn}(\text{C}_3\text{H}_7\text{ON}_2)]^+$ are given in the Supporting Information.

The lowest energy pathway for ammonia loss (Figure 7) from $[\text{Zn}(\text{C}_3\text{H}_7\text{ON}_2)]^+$ was found to occur from the amide group. From $[\text{Zn}(\text{C}_3\text{H}_7\text{ON}_2)]^+$, proton transfer from the N to N_s site occurs, passing through $\text{TS}_{1\text{D}}$. This transfer results in the formation of the NH_3 leaving group, as shown in $\text{INT}_{1\text{D}}$, thus

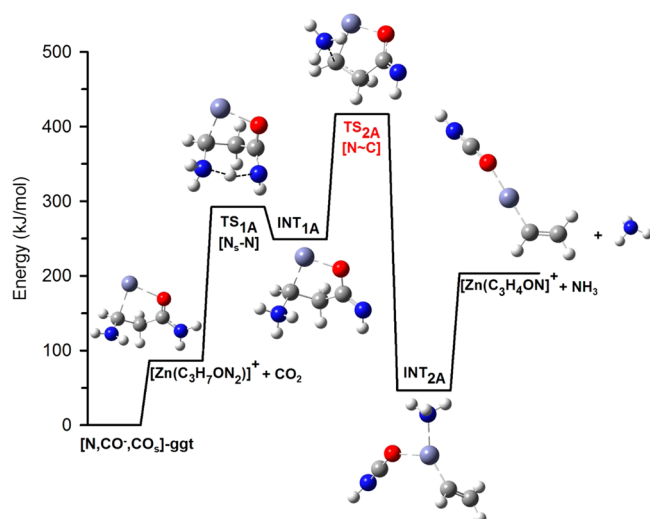


Figure 8. Reaction coordinate for ammonia loss via the backbone amino group from $[\text{Zn}(\text{C}_3\text{H}_7\text{ON}_2)]^+$ calculated at the MP2(full)/6-311+G(2d,2p) level of theory, using B3LYP/6-311+G(d,p) geometry optimizations. Structures for intermediates lie below the reaction coordinate, and those for TSs lie above. Dashed lines (gray) indicate M–L bonds. Dotted lines (black) indicate bonds being broken or formed for transition states.

elongating the C–N_s amide bond by ~0.2 Å. Further elongation of this bond results in rupture via TS_{2D}. The complex formed, INT_{2D}, is stabilized by the ammonia remaining loosely bound to the system via hydrogen bonding. Simple dissociation of this complex can lead to $[\text{Zn}(\text{C}_3\text{H}_4\text{ON})]^+ + \text{NH}_3$, which requires 250–331 kJ/mol relative to $[\text{Zn}(\text{Asn-H})]^+$. An interesting observation made here is that the proton transfer of TS_{1D} results in the stabilization of INT_{1D} in such a way (NH₃⁺ formation) that the charge is now located on the ligand, rather than residing on zinc. Thus, along the PES, Zn behaves as a neutral rather than its dication counterpart, as is evident from the longer M–L interactions and (although this is difficult to ascertain from the orientation of the structures shown) the fact that Zn lies out of the plane of the ligand. Zn–L bond lengths are given in Figure 7, where it can be seen that interactions involving neutral zinc are 0.3–1.2 Å longer than those with the dication counterpart. The relatively high

energies found here for deamidation are then consistent with inefficient dissociation found experimentally for the IRMPD process of $[\text{Zn}(\text{Asn-H})]^+$.

Alternatively, ammonia can be lost from the backbone amino group, as illustrated in Figure 8. Here, proton transfer from N_s to N results in the formation of the NH₃ leaving group, thus increasing the N–C_α bond distance. Further elongation of this bond results in bond rupture as the complex passes through rate-limiting TS_{2A} (348–417 kJ/mol above $[\text{Zn}(\text{Asn-H})]^+$). This motion is stabilized by the formation of INT_{2A}, where the Zn²⁺ center becomes tridentate, binding to HC=CH₂, NH₃, and O=C=NH (given in order of increasing M–L bond distances). Simple dissociation of this complex can lead to $[\text{Zn}(\text{C}_3\text{H}_4\text{ON})]^+ + \text{NH}_3$, which requires 140–216 kJ/mol relative to $[\text{Zn}(\text{Asn-H})]^+$. The results of Figures 7 and 8 make it apparent that the energetically favored reaction is deamidation of the complex, as the product asymptote for deamidation is 56–109 kJ/mol lower in energy than the rate-limiting transition state (TS_{2A}) for deamidation. Another interesting observation is that Zn–L distances observed for deamidation are much longer than those observed in the amino NH₃ loss pathway. This observation is consistent with the findings for $[\text{Zn}(\text{Gln-H})]^+$ deamidation where the Zn metal center dissociates as a neutral prior to deamidation. Thus, although deamidation in the current study can still occur with Zn binding, there is still a tendency to weaken the metal–ligand interactions to induce a more facile reaction pathway for deamidation.

Deamidation Pathways for CdCl⁺(Asn). For the CdCl⁺(Asn) complex, the most plausible deamidation pathway would likely involve hydrogen transfer from the carboxylic acid group to the amide NH₂, similar to the mechanism detailed for deamidation of protonated and sodiated Asn.^{6,8} These studies concluded that deamidation resulted in the formation of 3-amino succinic anhydride (aSA), paralleling the mechanism proposed in biological systems where the deamidation process is believed to proceed through a succinimide intermediate. Deviations from this pathway arise when the additional CO loss is considered, an important aspect of the dissociation pathways exhibited in the current study, where only concomitant loss of NH₃ + CO is observed. For H⁺(Asn), secondary CO loss was observed at considerably higher energy than deamidation,⁸ and

Table 1. Relative Energies (0 K) and Free Energies (298 K) of Major Reaction Species Forming *m/z* 134 from $[\text{Zn}(\text{Asn-H})]^+$ ^a

reaction	structure	B3LYP/GD3BJ ^b	B3P86	MP2(full)
deamidation	$[\text{N}, \text{CO}^-, \text{CO}_s]\text{-gggt}$	0.0 (0.0)/0.0 (0.0)	0.0 (0.0)	0.0 (0.0)
	$[\text{Zn}(\text{C}_3\text{H}_7\text{ON}_2)]^+ + \text{CO}_2$	33.2 (35.6)/57.6 (60.0)	68.8 (71.2)	86.5 (88.9)
	TS _{1D} [N–N _s]	102.8 (109.8)/132.2 (139.1)	157.1 (164.0)	164.6 (171.6)
	INT _{1D}	108.0 (112.3)/134.3 (138.5)	165.3 (169.6)	169.6 (173.9)
	TS _{2D} [N _s –C]	202.8 (212.6)/240.9 (250.7)	281.9 (291.7)	254.1 (263.9)
	INT _{2D}	192.0 (202.4)/229.3 (239.8)	267.2 (277.7)	251.1 (261.6)
	$[\text{Zn}(\text{C}_3\text{H}_4\text{ON})]^+ + \text{CO}_2 + \text{NH}_3$	250.4 (225.6)/294.0 (269.3)	331.2 (306.4)	307.4 (282.7)
amino loss	$[\text{N}, \text{CO}^-, \text{CO}_s]\text{-gggt}$	0.0 (0.0)/0.0 (0.0)	0.0 (0.0)	0.0 (0.0)
	$[\text{Zn}(\text{C}_3\text{H}_7\text{ON}_2)]^+ + \text{CO}_2$	33.2 (35.6)/57.6 (60.0)	68.8 (71.2)	86.5 (88.9)
	TS _{1A}	273.3 (271.5)/290.2 (288.5)	287.4 (285.7)	292.2 (290.5)
	INT _{1A}	230.2 (231.2)/251.1 (252.2)	254.8 (255.9)	248.9 (250.0)
	TS _{2A}	348.1 (352.0)/368.2 (372.1)	387.1 (391.1)	416.5 (420.4)
	INT _{2A}	3.5 (15.6)/39.7 (51.8)	65.1 (77.2)	46.5 (58.6)
	$[\text{Zn}(\text{C}_3\text{H}_4\text{ON})]^+ + \text{CO}_2 + \text{NH}_3$	145.0 (123.4)/193.1 (171.5)	216.1 (194.5)	203.3 (181.8)

^aRelative single point energies and free energies in parentheses calculated at the level of theory indicated using a 6-311+G(2d,2p) basis set.

^bEmpirical dispersion corrected B3LYP-GD3BJ values are given in bold.

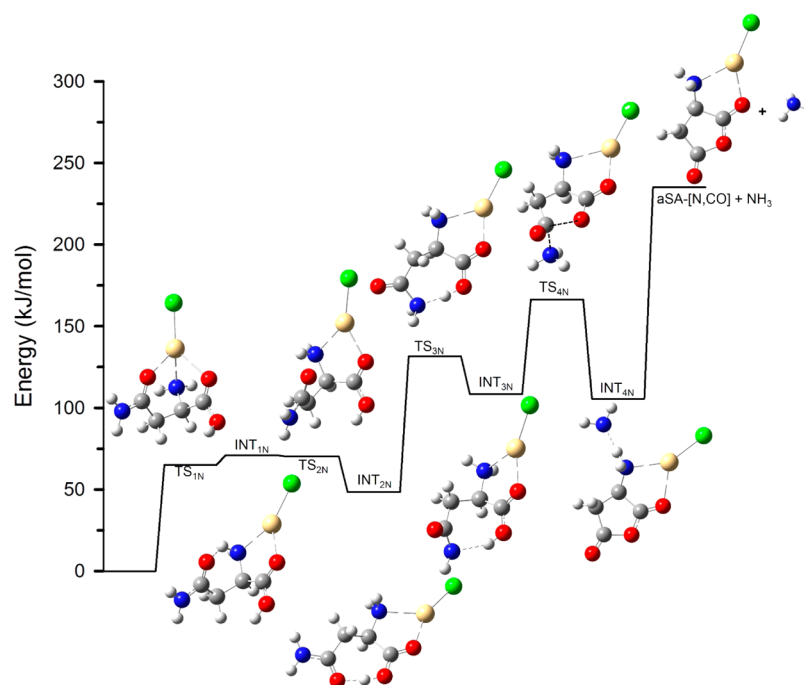


Figure 9. Reaction coordinate for aSA-[N,CO] formation from CdCl⁺(Asn) calculated at the MP2(full)/def2-TZVPP level of theory from B3LYP/def2-TZVP geometry optimizations. Structures for intermediates lie below the reaction coordinate, and those for TSs lie above. Dashed lines (gray) indicate hydrogen bonds (up to 2.5 Å). Dotted lines (black) indicate bonds being broken or formed for transition states.

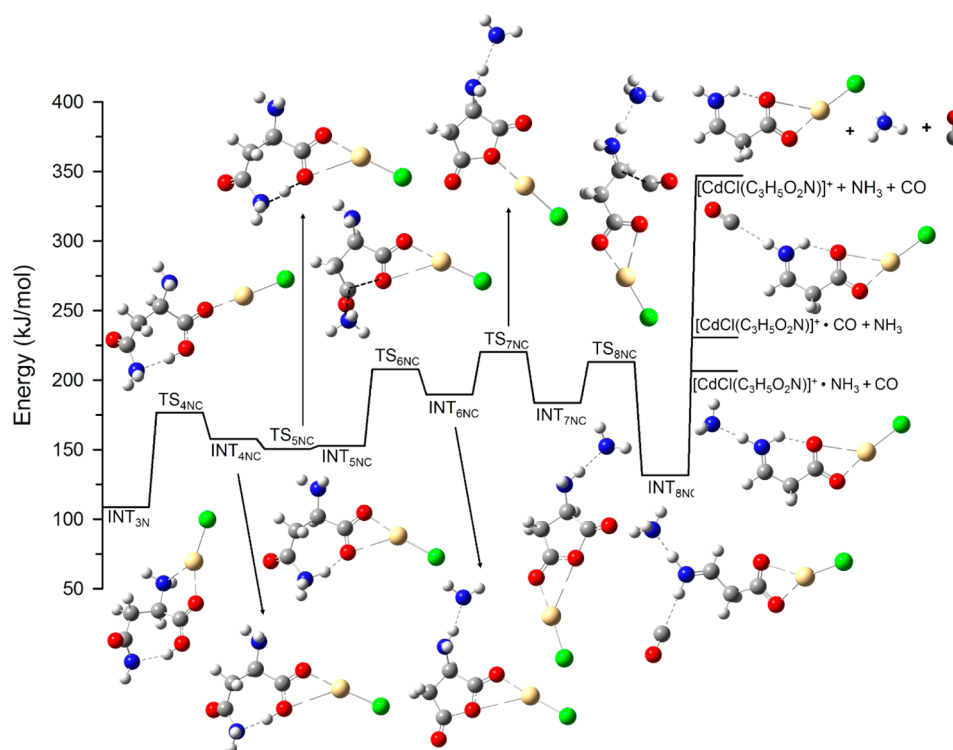


Figure 10. Reaction coordinates for the concomitant NH₃ and CO loss from CdCl⁺(Asn) calculated at the MP2(full)/def2-TZVPP//B3LYP/def2-TZVP level of theory. Structures for intermediates lie below the reaction coordinate, and those for TSs lie above. Dashed lines (gray) indicate hydrogen bonds (up to 2.5 Å). Dotted lines (black) indicate bonds being broken or formed for transition states.

for Na⁺(Asn), no CO loss was observed via TCID,⁶ even though energies up to 480 kJ/mol (5.0 eV) were monitored. Here, we explore the pathways for concomitant loss as well as the possibility of primary ammonia loss (Figure 9), followed by the sequential loss of CO (see the Supporting Information).

The possibility that CH₃NO is lost as formamide was also explored, although no reasonable pathway could be found. Instead, any pathway that could conceivably lead to loss of formamide led to preferential formation of H₂N–CO–NH₂. Therefore, the most plausible pathway leading to the formation

Table 2. Relative Energies (0 K) and Free Energies (298 K) of Major Reaction Species Forming the aSA Intermediate from CdCl⁺(Asn)^a

structure	B3LYP/GD3BJ ^b	B3P86	MP2(full)
[N, CO, CO _s]-tggt	0.0 (0.0)/ 0.0 (0.0)	0.0 (0.0)	0.0 (0.0)
TS _{1N}	62.6 (59.9)/ 62.0 (59.3)	63.6 (60.9)	65.1 (62.4)
INT _{1N}	63.5 (61.3)/ 66.1 (63.9)	63.7 (61.6)	70.9 (68.7)
TS _{2N}	63.8 (59.7)/ 65.8 (61.6)	64.6 (60.4)	70.2 (66.1)
INT _{2N}	32.5 (29.1)/ 38.6 (35.2)	29.7 (26.3)	48.4 (45.0)
TS _{3N}	121.8 (117.2)/ 126.8 (122.1)	120.5 (115.8)	131.5 (126.9)
INT _{3N}	100.2 (97.3)/ 103.0 (100.0)	100.5 (97.6)	108.4 (105.5)
TS _{4N} [OH–N _s], [N _s –C–O]	159.2 (157.1)/ 163.8 (161.6)	161.6 (159.5)	166.4 (164.2)
INT _{4N} , aSA _(NH-NH₃)	93.9 (94.4)/ 105.7 (106.2)	98.2 (98.6)	105.6 (106.1)
aSA-[N,CO] + NH ₃	167.7 (159.0)/ 188.4 (153.6)	177.4 (142.6)	235.1 (200.3)

^aRelative single point energies and free energies in parentheses calculated at the level of theory indicated using a def2-TZVPP basis set and SDD ECP for Cd. ^bEmpirical dispersion corrected B3LYP-GD3BJ values are given in bold.

Table 3. Relative Energies (0 K) and Free Energies (298 K) of Major Reaction Species Forming *m/z* 236 via (NH₃ + CO) Loss from CdCl⁺(Asn)^a

structure	B3LYP/GD3BJ ^b	B3P86	MP2(full)
[N, CO, CO _s]-tggt	0.0 (0.0)/ 0.0 (0.0)	0.0 (0.0)	0.0 (0.0)
TS _{1N}	62.6 (59.9)/ 62.0 (59.3)	63.6 (60.9)	65.1 (62.4)
INT _{1N}	63.5 (61.3)/ 66.1 (63.9)	63.7 (61.6)	70.9 (68.7)
TS _{2N}	63.8 (59.7)/ 65.8 (61.6)	64.6 (60.4)	70.2 (66.1)
INT _{2N}	32.5 (29.1)/ 38.6 (35.2)	29.7 (26.3)	48.4 (45.0)
TS _{3N}	121.8 (117.2)/ 126.8 (122.1)	120.5 (115.8)	131.5 (126.9)
INT _{3N}	100.2 (97.3)/ 103.0 (100.0)	100.5 (97.6)	108.4 (105.5)
TS _{4NC}	155.5 (152.0)/ 168.4 (165.0)	161.3 (157.9)	176.7 (173.3)
INT _{4NC}	137.9 (136.1)/ 149.7 (147.9)	142.0 (140.3)	157.6 (155.8)
TS _{5NC}	135.0 (132.2)/ 146.6 (143.8)	136.5 (133.7)	150.6 (147.8)
INT _{5NC}	136.9 (135.7)/ 148.0 (146.8)	141.8 (140.5)	152.7 (151.4)
TS _{6NC}	186.6 (187.7)/ 202.0 (203.2)	200.5 (201.6)	207.7 (208.8)
INT _{6NC}	159.2 (162.6)/ 182.3 (185.7)	172.8 (176.2)	189.6 (193.0)
TS _{7NC}	197.6 (199.3)/ 215.6 (217.3)	213.6 (215.3)	220.2 (221.9)
INT _{7NC}	153.2 (156.5)/ 176.4 (179.7)	167.4 (170.7)	183.5 (186.8)
TS _{8NC}	173.0 (177.1)/ 196.4 (200.5)	200.4 (204.5)	213.0 (217.1)
INT _{8NC}	94.6 (94.2)/ 120.7 (120.3)	139.9 (139.6)	131.5 (131.2)
[CdCl(C ₃ H ₅ O ₂ N)] ⁺ ·CO	100.4 (105.5)/ 137.4 (142.5)	145.7 (150.8)	208.5 (213.6)
[CdCl(C ₃ H ₅ O ₂ N)] ⁺ ·NH ₃	139.7 (113.1)/ 176.3 (149.7)	188.7 (162.0)	232.7 (206.0)
[CdCl(C ₃ H ₅ O ₂ N)] ⁺ + NH ₃ + CO	185.6 (154.6)/ 228.2 (197.3)	236.0 (205.1)	347.0 (316.1)

^aRelative single point energies and free energies in parentheses calculated at the level of theory indicated using a def2-TZVPP basis set and SDD ECP for Cd. ^bEmpirical dispersion corrected B3LYP-GD3BJ values are given in bold.

of CdCl⁺(C₃H₅O₂N) is the concomitant loss of (NH₃ + CO), as shown in Figure 10.

The PES showing the loss of ammonia to form CdCl⁺(aSA) is given in Figure 9, with energies of all reaction species given in Table 2. The first elementary step involves rotation of the ∠CCO³H dihedral angle such that the hydrogen bond of the carboxylic acid is broken, thus allowing a more facile proton transfer to N_s to form the NH₃ leaving group. To induce this proton transfer, a series of ∠CCCN dihedral angle rotations results in the decreased distance between N_s and the hydrogen of the carboxylic acid in INT_{3N}. Proton transfer occurs as the complex passes through TS_{4N}, characterized by concerted motions of NH₃ formation, C–NH₃ bond rupture, and ring closure. (Here, IRC calculations confirm the identity of TS_{4N} to ensure that there was not another TS leading to the formation of the NH₃ leaving group.) This TS leads to formation of CdCl⁺(aSA)[N, CO]_(NH-NH₃) (168–235 kJ/mol higher in energy than the ground conformer), in which the subscript indicates the ammonia is hydrogen bound to the NH group.

This sequence of steps parallels those found previously for deamidation of Asn cationized by Na⁺ and H⁺.^{6,8}

Here, we observe concomitant (NH₃ + CO) loss such that deamidation alone is not observed. Thus, dissociation of CdCl⁺(Asn) would appear to follow a pathway in which deamidation occurs at sufficiently low energies that sequential CO loss does not require much if any additional energy. In comparing the results obtained from TCID and IRMPD studies, however, it should be acknowledged that the high-energy single collisions of TCID are more likely to produce entropically favored products, whereas the multiple low-energy collisional processes used to induce deamidation in the spectroscopic study should yield enthalpically favored products. Thus, the different experimental conditions may allow for alternate pathways for deamidation than the pathways paralleling the TCID deamidations of H⁺(Asn) and Na⁺(Asn).

Our exploration of the PES for (NH₃ + CO) loss is shown in Figure 10, with relative energies given in Table 3. Here, the first three elementary steps are equivalent to the pathway given in

Figure 9 for $\text{CdCl}^+(\text{aSA})[\text{N}, \text{CO}]$ formation. From $\text{INT}_{3\text{N}}$, rotation of the $\angle\text{CdOCO}$ dihedral angle from trans to cis (passing through gauche $\text{TS}_{4\text{NC}}$) results in the formation of $\text{INT}_{4\text{NC}}$ where heavy metal binding occurs at the oxygen sites of the carboxylic acid, $[\text{COOH}]$. From here, proton transfer to the amide NH_2 group can occur facily, yielding the zwitterionic $\text{INT}_{5\text{NC}}$, $[\text{CO}_2^-]$, in which the NH_3 leaving group is formed. Elongation of the C– NH_3 bond over $\text{TS}_{6\text{NC}}$ results in the concerted motions of bond rupture and aSA formation, where stabilization of these motions results in $\text{INT}_{6\text{NC}}$, $\text{CdCl}^+(\text{aSA})[\text{CO}, \text{O}]_{(\text{NH}\cdot\text{NH}_3)}$, where the ammonia is hydrogen bonded to the amine group. Next, CdCl^+ migrates to break the $[\text{CO}, \text{O}]$ interaction of the carboxylic acid oxygens and reform the analogous interaction with the carbonyl oxygen of the side chain. Although $\text{INT}_{7\text{NC}}$ is 5–6 kJ/mol lower in energy than $\text{INT}_{6\text{NC}}$, $\text{TS}_{7\text{NC}}$ is sufficiently high in energy (198–220 kJ/mol) that this is the rate-limiting TS at the B3LYP level of theory. We also explored the possibility of forming $\text{INT}_{7\text{NC}}$ by CdCl^+ migration to the side-chain carbonyl prior to aSA formation, but no such pathway could be isolated. From $\text{INT}_{7\text{NC}}$, decarbonylation can occur from the backbone carbonyl adjacent to the nitrogen site by elongation of the NC–CO bond leading to $\text{TS}_{8\text{NC}}$. This motion yields $\text{INT}_{8\text{NC}}$, where the NH_3 and CO ligands remain hydrogen bound to the complex at the terminal NH_2 site. Again, this complex is zwitterionic with positive charge on the nitrogen and delocalized negative charge on the carboxylate group, a species that parallels that found in the $\text{H}^+(\text{Asn})$ study. (Notably, decarbonylation from $\text{INT}_{6\text{NC}}$ is much higher in energy than the pathway shown because the final product formed is much less stable.) From this intermediate, CO can be lost most easily, as it requires only 6–77 kJ/mol (100–209 kJ/mol above the reactants) and NH_3 loss requires about 30 kJ/mol more (140–233 kJ/mol above reactants). Loss of both ligands yields $\text{CdCl}^+(\text{C}_3\text{H}_5\text{O}_2\text{N}) + \text{NH}_3 + \text{CO}$, 186–347 kJ/mol relative to the ground reactant conformer. Importantly, the energy of $\text{TS}_{8\text{NC}}$ (173–213 kJ/mol) is the lowest energy TS for decarbonylation that we have found, suggesting that the complex is most likely to lose CO via this pathway. Alternate pathways (where metal binding is taking place at $[\text{N}, \text{CO}]$ or $[\text{CO}, \text{O}]$ of the backbone) were located, although each of these TSs were significantly higher in energy. Select pathways exploring these TSs are given in the [Supporting Information](#).

From an energetic point of view, primary deamidation via the loose, phase-space limit TS of Figure 9 (168–188 kJ/mol) should occur at lower energies relative to the concomitant pathway via $\text{TS}_{7\text{NC}}$ detailed in Figure 10 (198–216 kJ/mol) according to the DFT level of theory. However, MP2(full) theory indicates that $\text{TS}_{7\text{NC}}$ (220 kJ/mol) is lower than the deamidation products of Figure 9 (235 kJ/mol), such that these pathways could be competitive. Once over $\text{TS}_{7\text{NC}}$, the system should preferentially lose CO first, and require additional energy to lose NH_3 as well. Significantly, although the pathways shown in Figures 9 and 10 may be competitive, neither pathway clearly explains why the concomitant loss of ($\text{NH}_3 + \text{CO}$) is observed rather than observing loss of just NH_3 (Figure 9) or CO (Figure 10).

Select higher energy conformers of $\text{CdCl}^+(\text{C}_3\text{H}_5\text{O}_2\text{N})$ are given in the [Supporting Information](#) (Figure S2). Here, several additional pathways were found for the loss of ($\text{NH}_3 + \text{CO}$) from $\text{CdCl}^+(\text{Asn})$, but all lie at higher energy than that shown

in Figure 10, as detailed in the [Supporting Information](#) (Figures S3–S6).

From a structural perspective, comparison of the geometric analysis of both $\text{Zn}^{2+}/\text{Cd}^{2+}$ Asn and $\text{Zn}^{2+}/\text{Cd}^{2+}$ Gln systems is particularly helpful in analyzing the deamidation patterns exhibited by each of the complexes. Here, the most interesting observation is that Zn + CO_2 dissociation from $[\text{Zn}(\text{Gln}\text{--}\text{H})]^+$ occurs prior to deamidation, whereas, from $[\text{Zn}(\text{Asn}\text{--}\text{H})]^+$, loss of CO_2 occurs before ammonia loss but the Zn^{2+} metal center is still bound. On the basis of M–N, M–O, and M–CO_s distances, very similar lengths were found for the deprotonated Asn (2.06, 1.89, and 1.96 Å, respectively) and Gln (2.06, 1.88, and 1.93 Å, respectively) complexes with Zn^{2+} .¹⁵ The most noticeable difference in the geometric parameters is the significantly smaller $\angle\text{OMO}_s$ angle in the current Asn study (110.7° for Asn, compared with 125.6° for Gln). This effect is attributed to the extra carbon in the backbone of Gln, which increases this angle. Although the additional carbon allows for increased flexibility along the backbone, the more constrained $\angle\text{OMO}_s$ angle in the Asn complex appears to help maintain a compact conformation that is more suitable for cyclization (where the ability to form the cyclic succinimide structure is particularly important for the deamidation process). A similar trend in smaller $\angle\text{XMY}_s$ and $\angle\text{OMY}_s$ angles is observed in the Cd^{2+} system as well, although the differences are not as pronounced. Such small differences are consistent with the dissociation patterns observed, where Cd^{2+} remains more loosely bound (compared with Zn^{2+}) to the system in both Asn and Gln studies. Here, the distinct difference in deamidation pathways for both systems arises from the fact that deamidation was observed as the only primary loss of the Cd^{2+} Gln system,¹⁵ whereas the simultaneous loss of NH_3 and CO was detected in the current study as the only dissociation product of $\text{CdCl}^+(\text{Asn})$.

CONCLUSIONS

IRMPD action spectra for complexes of asparagine cationized with Zn^{2+} and Cd^{2+} were measured in the region of 1000–1850 cm^{-1} and were compared to calculated IR spectra at the B3LYP/6-311+G(d,p) and B3LYP/def2-TZVP levels of theory, respectively. For both $[\text{Zn}(\text{Asn}\text{--}\text{H})]^+$ and $\text{CdCl}^+(\text{Asn})$, the theoretically determined ground conformer is found to reproduce the experimental spectra well. The $[\text{N}, \text{CO}^-, \text{CO}_s]$ -ggg conformer of the $[\text{Zn}(\text{Asn}\text{--}\text{H})]^+$ complex is confirmed to be the complex present experimentally, with no major contributions from higher lying conformers. For the $\text{CdCl}^+(\text{Asn})$ complex, the experimental IRMPD spectrum was predicted best by the $[\text{N}, \text{CO}, \text{CO}_s]$ -tggt conformer.

The analysis regarding the changes in vibrational modes and geometric parameters also provides valuable information about the binding strength of the metal center within the complex, a characterization instrumental in determining the metal dependence of these and other biologically relevant systems. The shorter M–O and M–X distances of the $[\text{Zn}(\text{Asn}\text{--}\text{H})]^+$ complex should characteristically lead to stronger metal–amino acid binding compared to binding observed in $\text{CdCl}^+(\text{Asn})$. This weaker binding along with the less constrained dihedral angles in the $\text{CdCl}^+(\text{Asn})$ complex appears to facilitate the formation of a cyclic succinic anhydride structure that is necessary for deamidation to occur. We have previously correlated these findings (regarding the ability for movement within the complex as well as metal chelation throughout the dissociation process) to the observation of

differing pathways for deamidation, as the Zn^{2+} center dissociates prior to deamidation in the Zn^{2+} Gln system. In the current study, however, deamidation was observed with the Zn^{2+} center intact (although long M–L interactions were observed and, here, Zn acts as a neutral rather than a dication after CO_2 loss), although no cyclization was determined to occur.

The characteristic vibrational modes in the $[\text{Zn}(\text{Asn}-\text{H})]^+$ and $\text{CdCl}^+(\text{Asn})$ spectra also provide valuable information with respect to the metal dependence of the system (as given by the band shifts observed in our spectral results), although some contributions to those shifts arise from the inherent difference in binding between Zn^{2+} and anionic (Asn–H) versus CdCl^+ and neutral Asn. Overall, the results presented here provide valuable fundamental information for the continuation of our metal-amino acid studies, specifically regarding the metal dependence of biologically important systems. Specifically, the different deamidation patterns observed between the Asn and Gln systems are an important aspect to evaluate in other larger, more biologically relevant systems.

■ ASSOCIATED CONTENT

📄 Supporting Information

The Supporting Information is available free of charge on the ACS Publications website at DOI: 10.1021/acs.jpccb.6b10326.

Additional information including vibrational frequencies and IR intensities of low energy conformers, conformers of $[\text{Zn}(\text{C}_3\text{H}_7\text{ON})]^+$ and $\text{CdCl}^+(\text{C}_3\text{H}_5\text{O}_2\text{N})$, and alternate PESs (PDF)

■ AUTHOR INFORMATION

Corresponding Author

*E-mail: armentrout@chem.utah.edu.

ORCID

P. B. Armentrout: 0000-0003-2953-6039

Notes

The authors declare no competing financial interest.

■ ACKNOWLEDGMENTS

Financial support for this work was provided by the National Science Foundation, grants CHE-1359769 and OISE-1357887. The skillful assistance of the FELIX staff is gratefully acknowledged. In addition, a grant of computer time from the Center of High Performance Computing at the University of Utah is greatly appreciated.

■ REFERENCES

- (1) Robinson, N. E.; Robinson, A. B. Molecular Clocks. *Proc. Natl. Acad. Sci. U. S. A.* **2001**, *98*, 944–949.
- (2) Nilsson, M. R.; Driscoll, M.; Raleigh, D. P. Low Levels of Asparagine Deamidation Can Have a Dramatic Effect on Aggregation of Amyloidogenic Peptides: Implications for the Study of Amyloid Formation. *Protein Sci.* **2002**, *11*, 342–349.
- (3) Robinson, N. E.; Robinson, A. B. Deamidation of Human Proteins. *Proc. Natl. Acad. Sci. U. S. A.* **2001**, *98*, 12409–12413.
- (4) Robinson, N. E.; Robinson, A. B. *Molecular Clocks: Deamidation of Asparaginyl and Glutaminyl Residues in Peptides and Proteins*; Althouse Press: Cave Junction, OR, 2004.
- (5) Heaton, A. L.; Bowman, V. N.; Oomens, J.; Steill, J. D.; Armentrout, P. B. Infrared Multiple Photon Dissociation Spectroscopy of Cationized Asparagine: Effects of Alkali-Metal Cation Size on Gas-Phase Conformation. *J. Phys. Chem. A* **2009**, *113*, 5519–5530.

- (6) Heaton, A. L.; Moision, R. M.; Armentrout, P. B. Experimental and Theoretical Studies of Sodium Cation Interactions with the Acidic Amino Acids and Their Amide Derivatives. *J. Phys. Chem. A* **2008**, *112*, 3319–3327.

- (7) Heaton, A. L.; Armentrout, P. B. Experimental and Theoretical Studies of Potassium Cation Interactions with the Acidic Amino Acids and Their Amide Derivatives. *J. Phys. Chem. B* **2008**, *112*, 12056–12065.

- (8) Heaton, A. L.; Armentrout, P. B. Thermodynamics and Mechanism of Protonated Asparagine Decomposition. *J. Am. Soc. Mass Spectrom.* **2009**, *20*, 852–866.

- (9) Iuchi, S. Three Classes of C_2H_2 Zinc Finger Proteins. *Cell. Mol. Life Sci.* **2001**, *58*, 625–635.

- (10) Laity, J. H.; Lee, B. M.; Wright, P. E. Zinc Finger Proteins: New Insights into Structural and Functional Diversity. *Curr. Opin. Struct. Biol.* **2001**, *11*, 39–46.

- (11) Malgieri, G.; Zaccaro, L.; Leone, M.; Bucci, E.; Esposito, S.; Baglivo, I.; del Gatto, A.; Russo, L.; Scandurra, R.; Pedone, P. V.; et al. Zinc to Cadmium Replacement in the A. Thaliana Superman Cys_2His_2 Zinc Finger Induces Structural Rearrangements of Typical DNA Base Determinant Positions. *Biopolymers* **2011**, *95*, 801–810.

- (12) Malgieri, G.; Palmieri, M.; Esposito, S.; Maione, V.; Russo, L.; Baglivo, I.; de Paola, I.; Milardi, D.; Diana, D.; Zaccaro, L.; et al. Zinc to Cadmium Replacement in the Prokaryotic Zinc-Finger Domain. *Metallomics* **2014**, *6*, 96–104.

- (13) Hofstetter, T. E.; Howder, C.; Berden, G.; Oomens, J.; Armentrout, P. B. Structural Elucidation of Biological and Toxicological Complexes: Investigation of Monomeric and Dimeric Complexes of Histidine with Multiply Charged Transition Metal (Zn and Cd) Cations Using IR Action Spectroscopy. *J. Phys. Chem. B* **2011**, *115*, 12648–12661.

- (14) Coates, R. A.; McNary, C. P.; Boles, G. C.; Berden, G.; Oomens, J.; Armentrout, P. B. Structural Characterization of Gas-Phase Cysteine and Cysteine Methyl Ester Complexes with Zinc and Cadmium Dications by Infrared Multiple Photon Dissociation Spectroscopy. *Phys. Chem. Chem. Phys.* **2015**, *17*, 25799–25808.

- (15) Boles, G. C.; Coates, R. A.; Berden, G.; Oomens, J.; Armentrout, P. B. Experimental and Theoretical Investigations of Infrared Multiple Photon Dissociation Spectra of Glutamine Complexes with Zn^{2+} and Cd^{2+} . *J. Phys. Chem. B* **2015**, *119*, 11607–11617.

- (16) Coates, R. A.; Boles, G. C.; McNary, C. P.; Berden, G.; Oomens, J.; Armentrout, P. B. Zn^{2+} and Cd^{2+} Cationized Serine Complexes: Infrared Multiple Photon Dissociation Spectroscopy and Density Functional Theory Investigations. *Phys. Chem. Chem. Phys.* **2016**, *18*, 22434–22445.

- (17) Oepts, D.; van der Meer, A. F. G.; van Amersfoort, P. W. The Free-Electron-Laser User Facility Felix. *Infrared Phys. Technol.* **1995**, *36*, 297–308.

- (18) Valle, J. J.; Eyler, J. R.; Oomens, J.; Moore, D. T.; van der Meer, A. F. G.; von Helden, G.; Meijer, G.; Hendrickson, C. L.; Marshall, A. G.; Blakney, G. T. Free Electron Laser-Fourier Transform Ion Cyclotron Resonance Mass Spectrometry Facility for Obtaining Infrared Multiphoton Dissociation Spectra of Gaseous Ions. *Rev. Sci. Instrum.* **2005**, *76*, 023103.

- (19) Polfer, N. C.; Oomens, J.; Moore, D. T.; von Helden, G.; Meijer, G.; Dunbar, R. C. Infrared Spectroscopy of Phenylalanine $\text{Ag}(\text{I})$ and $\text{Zn}(\text{II})$ Complexes in the Gas Phase. *J. Am. Chem. Soc.* **2006**, *128*, 517–525.

- (20) Polfer, N. C.; Oomens, J. Reaction Products in Mass Spectrometry Elucidated with Infrared Spectroscopy. *Phys. Chem. Chem. Phys.* **2007**, *9*, 3804–3817.

- (21) Marshall, A. G.; Wang, T. C. L.; Ricca, T. L. Tailored Excitation for Fourier Transform Ion Cyclotron Resonance Mass Spectrometry. *J. Am. Chem. Soc.* **1985**, *107*, 7893–7897.

- (22) Guan, S. H.; Marshall, A. G. Stored Waveform Inverse Fourier Transform (SWIFT) Ion Excitation in Trapped-Ion Mass Spectrometry: Theory and Applications. *Int. J. Mass Spectrom. Ion Processes* **1996**, *157–158*, 5–37.

(23) Lemaire, J.; Boissel, P.; Heninger, M.; Mauclaire, G.; Bellec, G.; Hestdagh, H.; Simon, A.; Le Caer, S.; Ortega, J. M.; Glotin, F.; et al. Gas Phase Infrared Spectroscopy of Selectively Prepared Ions. *Phys. Rev. Lett.* **2002**, *89*, 273002.

(24) Dunbar, R. C. Infrared Radiative Cooling of Isolated Polyatomic Molecules. *J. Chem. Phys.* **1989**, *90*, 7369–7375.

(25) Frisch, M. J.; Trucks, G. W.; Schlegel, H. B.; Scuseria, G. E.; Robb, M. A.; Cheeseman, J. R.; Scalmani, G.; Barone, V.; Mennucci, B.; Petersson, G. A.; et al. *Gaussian 09*, revision D.01; Gaussian, Inc.: Wallingford, CT, 2009.

(26) Weigend, F.; Ahlrichs, R. Def2-SVP Basis Sets. *Phys. Chem. Chem. Phys.* **2005**, *7*, 3297–3305.

(27) Andrae, D.; Haeussermann, U.; Dolg, M.; Stoll, H.; Preuss, H. Energy-Adjusted Ab Initio Pseudopotentials for the Second and Third Row Transition Elements. *Theor. Chim. Acta* **1990**, *77*, 123–141.

(28) Feller, D. The Role of Databases in Support of Computational Chemistry Calculations. *J. Comput. Chem.* **1996**, *17*, 1571–1586.

(29) Grimme, S.; Ehrlich, S.; Goerigk, L. Effect of the Damping Function in Dispersion Corrected Density Functional Theory. *J. Comput. Chem.* **2011**, *32*, 1456–1465.

(30) Polfer, N. C. Infrared Multiple Photon Dissociation Spectroscopy of Trapped Ions. *Chem. Soc. Rev.* **2011**, *40*, 2211–2221.

(31) Berglund, M.; Wieser, M. E. Isotopic Compositions of the Elements 2009. *Pure Appl. Chem.* **2011**, *83*, 397–410.

(32) Bush, M. F.; Oomens, J.; Saykally, R. J.; Williams, E. R. Alkali Metal Ion Binding to Glutamine and Glutamine Derivatives Investigated by Infrared Action Spectroscopy and Theory. *J. Phys. Chem. A* **2008**, *112*, 8578–8584.

(33) O'Brien, J. T.; Prell, J. S.; Steill, J. D.; Oomens, J.; Williams, E. R. Interactions of Mono- and Divalent Metal Ions with Aspartic and Glutamic Acid Investigated with IR Photodissociation Spectroscopy and Theory. *J. Phys. Chem. A* **2008**, *112*, 10823–10830.

(34) Oomens, J.; Steill, J. D.; Redlich, B. Gas-Phase IR Spectroscopy of Deprotonated Amino Acids. *J. Am. Chem. Soc.* **2009**, *131*, 4310–4319.

(35) Oomens, J.; Sartakov, B. G.; Meijer, G.; von Helden, G. Gas-Phase Infrared Multiple Photon Dissociation Spectroscopy of Mass-Selected Molecular Ions. *Int. J. Mass Spectrom.* **2006**, *254*, 1–19.

(36) Citir, M.; Stennett, E. M. S.; Oomens, J.; Steill, J. D.; Rodgers, M. T.; Armentrout, P. B. Infrared Multiple Photon Dissociation Spectroscopy of Cationized Cysteine: Effects of Metal Cation Size on Gas-Phase Conformation. *Int. J. Mass Spectrom.* **2010**, *297*, 9–17.

(37) Citir, M.; Hinton, C. S.; Oomens, J.; Steill, J. D.; Armentrout, P. B. Infrared Multiple Photon Dissociation Spectroscopy of Cationized Histidine: Effects of Metal Cation Size on Gas-Phase Conformation. *J. Phys. Chem. A* **2012**, *116*, 1532–1541.

(38) Oomens, J.; Moore, D. T.; Meijer, G.; von Helden, G. Infrared Multiple Photon Dynamics and Spectroscopy of Cationic Paba and Its Dehydroxylated Fragment Ion. *Phys. Chem. Chem. Phys.* **2004**, *6*, 710–718.

(39) Rodgers, M. T.; Armentrout, P. B.; Oomens, J.; Steill, J. D. Infrared Multiphoton Dissociation Spectroscopy of Cationized Threonine: Effects of Alkali-Metal Cation Size on Gas-Phase Conformation. *J. Phys. Chem. A* **2008**, *112*, 2258–2267.

(40) Armentrout, P. B.; Rodgers, M. T.; Oomens, J.; Steill, J. D. Infrared Multiphoton Dissociation Spectroscopy of Cationized Serine: Effects of Alkali-Metal Cation Size on Gas-Phase Conformation. *J. Phys. Chem. A* **2008**, *112*, 2248–2257.

(41) Carl, D. R.; Cooper, T. E.; Oomens, J.; Steill, J. D.; Armentrout, P. B. Infrared Multiple Photon Dissociation Spectroscopy of Cationized Methionine: Effects of Alkali-Metal Cation Size on Gas-Phase Conformation. *Phys. Chem. Chem. Phys.* **2010**, *12*, 3384–3398.

(42) Barth, A. The Infrared Absorption of Amino Acid Side Chains. *Prog. Biophys. Mol. Biol.* **2000**, *74*, 141–173.

(43) Joseph, J.; Jemmis, E. D. Red-, Blue-, or No-Shift in Hydrogen Bonds: A Unified Explanation. *J. Am. Chem. Soc.* **2007**, *129*, 4620–4632.